1 **Improved model of isoprene emissions in Africa using OMI satellite observations of**

2 **formaldehyde: implications for oxidants and particulate matter**

3 E. A. Marais[1,*], D. J. Jacob[1,2], A. Guenther[3], K. Chance[4], T. P. Kurosu[5], J. G. Murphy[6], C. E.

4 Reeves[7], H. O. T. Pye[8]

5 1. Earth and Planetary Sciences, Harvard University, Cambridge, MA, USA.

6 2. School of Engineering and Applied Sciences, Harvard University, Cambridge, MA, USA.

7 3. Pacific Northwest National Laboratory, Richland, WA, USA.

8 4. Harvard-Smithsonian Center for Astrophysics, Cambridge, MA, USA.

9 5. Earth Atmosphere Science, Jet Propulsion Laboratory, Pasadena, CA, USA.

10 6. Department of Chemistry, University of Toronto, Toronto, Canada.

11 7. School of Environmental Sciences, University of East Anglia, Norwich, UK.

12 8. National Exposure Research Laboratory, US EPA, Research Triangle Park, NC, USA.

13 *Now at School of Engineering and Applied Sciences, Harvard University, Cambridge, MA,

14 USA.

15

16 Corresponding author contact information:

17

18 Eloïse Ann Marais

19 Tel: +1-617-385-7834

20 Fax: +1-317-495-4551

21 Email: emarais@seas.harvard.edu

Abstract

We use a 2005-2009 record of isoprene emissions over Africa derived from OMI satellite observations of formaldehyde (HCHO) to better understand the factors controlling isoprene emission in the continent and evaluate the impact on atmospheric composition. OMI-derived isoprene emissions show large seasonality over savannas driven by temperature and leaf area index (LAI), and much weaker seasonality over equatorial forests driven by temperature. The commonly used MEGAN (version 2.1) global isoprene emission model reproduces this seasonality but is biased high, particularly for equatorial forests, when compared to OMI and relaxed-eddy accumulation measurements. Isoprene emissions in MEGAN are computed as the product of an emission factor E_o, LAI, and activity factors dependent on environmental variables. We use the OMI-derived emissions to provide improved estimates of E_o that are in good agreement with direct leaf measurements from field campaigns ($r = 0.55$, bias = -19%). The largest downward corrections to MEGAN E_o values are for equatorial forests and semi-arid environments, and this is consistent with latitudinal transects of isoprene over West Africa from the AMMA aircraft campaign. Total emission of isoprene in Africa is estimated to be 77 Tg C a^{-1}, compared to 104 Tg C a^{-1} in MEGAN. Simulations with the GEOS-Chem oxidant-aerosol model suggest that isoprene emissions increase mean surface ozone in West Africa by up to 8 ppbv, and particulate matter by up to 1.5 μg m^{-3}, due to coupling with anthropogenic influences.

41

1. Introduction

Isoprene is the dominant biogenic non-methane volatile organic compound (NMVOC)

emitted by vegetation, accounting for about 50% of global NMVOC emissions in current

inventories (Olivier et al,. 1996; Guenther et al., 2006). Isoprene affects the oxidative capacity of

the atmosphere through reaction with OH (Ren et al., 2008; Lelieveld et al., 2008) and as a

 precursor of O_3 (Trainer et al., 1987). It is also an important precursor for secondary organic

aerosols (SOA) (Claeys et al., 2004) and a temporary reservoir for nitrogen oxide radicals (NO_x

$\equiv NO + NO_2$) by formation of organic nitrates (Paulot et al., 2012). Isoprene thus has a range of

impacts on air quality and climate that need to be included in atmospheric composition models.

The widely used MEGAN global emission model (Guenther et al., 2006, 2012) indicates that

80% of global isoprene emission takes place in the tropics and 25% in Africa, but there are large

uncertainties in these estimates due to lack of data. In previous work we developed a method to

estimate isoprene emissions from Africa on the basis of observations of formaldehyde (HCHO)

from the OMI satellite instrument (Marais et al., 2012). Here we use our OMI-derived isoprene

emissions evaluated with local data to better understand the factors controlling isoprene

emissions in Africa, improve emission estimates for different African plant functional types

(PFTs), and assess the implications for atmospheric oxidants and aerosols.

Isoprene produced in the chloroplasts of plants is released to the atmosphere via the

stomata of leaves (Sharkey and Yeh, 2001). Above-canopy emission fluxes E_{ISOP} depend on

plant species, foliage density, leaf age, temperature, photosynthetically active radiation (PAR),

and water stress (Guenther et al., 1995). This is commonly represented in isoprene emission

models by multiplying an emission factor E_o defined for each PFT at standard conditions with an

3

64   ensemble of coefficients describing the sensitivity to local environmental variables. In the

65   MEGAN (version 2.1) inventory (Guenther et al., 2012) this is given as

66    $E_{\text{ISOP}} = E_o \times C_{\text{CE}} \times \text{LAI} \times \gamma_{\text{PAR}} \times \gamma_T \times \gamma_{\text{AGE}} \times \gamma_{\text{SM}}$ (1).

67   where LAI is the leaf area index (m^2 leaf surface per m^2 of Earth surface) and the dimensionless

68   activity factors γ describe the sensitivity to above-canopy radiation (PAR), air temperature (*T*),

69   leaf age distribution (AGE), and soil moisture (SM). The coefficient C_{CE} = 1.3 (m^2 Earth surface

70   per m^2 leaf surface) enforces E_{ISOP} = E_o under standard conditions, which for MEGAN are

71   defined as T = 303 K, PAR = 1000 µmol photons m^{-2} s^{-1}, a canopy with LAI = 5 m^2 m^{-2}, and leaf

72   age distribution of 80% mature, 10% growing, and 10% senescing leaves, and volumetric soil

73   moisture of 0.3 m^3 m^{-3}.

74   Isoprene emission data for African vegetation are very limited, and emission models

75   require extrapolation of data from other continents and across plant species (Guenther et al.,

76   2006; 2012). This can lead to substantial errors, as differences in isoprene fluxes within and

77   across plant species are large. Uncertainty in the distribution of land cover (PFT) adds to the

78   uncertainty (Pfister et al., 2008).

79   Space-based observations of HCHO, a high-yield oxidation product of isoprene, have

80   been used in a number of studies to infer isoprene emissions and evaluate inventories globally

81   (Shim et al., 2005; Stavrakou et al., 2009a; 2009b) and regionally in Southeast Asia (Fu et al.,

82   2007), South America (Barkley et al., 2008), North America (Palmer et al., 2003; 2006; Millet et

83   al., 2008), Europe (Dufour et al., 2009; Curci et al., 2010), and Africa (Marais et al., 2012).

84   These studies have confirmed temperature as the dominant factor controlling month-to-month

85   variability of isoprene emissions across North America (Palmer et al., 2006; Millet et al., 2008)

86   and Amazonia (Barkley et al., 2008). Leaf phenology and PAR were found to be additional

87 important drivers of isoprene emission seasonality in Amazonia (Barkley et al., 2008; 2009).

88 Stavrakou et al. (2009a) found that water stress reduces isoprene emissions in southern Africa

89 during the dry season. Here we use our previous work for Africa (Marais et al., 2012) to better

90 understand the factors controlling isoprene emissions across the African continent and evaluate

91 and improve the MEGANv2.1 emission inventory.

92

2. OMI-derived isoprene emissions in Africa

94   The derivation of isoprene emissions in Africa using OMI HCHO data is described in

95 Marais et al. (2012) and summarized briefly here. OMI is a UV/VIS solar backscatter instrument

96 on the Aura polar sun-synchronous satellite launched in 2004 (Levelt et al., 2006). It has a 13×24

97 km^2 nadir pixel resolution, daily global coverage through cross-track viewing, and 13:30 local

98 time (LT) overpass. HCHO slant columns are obtained from Version 2.0 (Collection 3) retrievals

99 for 2005–2009 (http://disc.sci.gsfc.nasa.gov/Aura/data-holdings/OMI/omhcho_v003.shtml).

100 They are corrected for instrument drift and converted to vertical columns using local air mass

101 factors (AMF) for the scattering atmosphere (Palmer et al., 2001) with vertical HCHO profiles

102 from the GEOS-Chem chemical transport model (CTM) v9-01-03 (http://www.geos-chem.org)

103 and scattering weights from the LIDORT radiative transfer model (Spurr et al., 2001).

104   HCHO enhancements over Africa primarily originate from isoprene emission, biomass

105 burning, and fuel combustion. Scenes affected by biomass burning are excluded on the basis of

106 MODIS satellite observations of fire counts and OMI satellite observations of aerosol absorption

107 optical depth (AAOD) (Torres et al., 2007). Scenes affected by gas flaring are excluded on the

108 basis of a specialized hotspot product from the AATSR satellite sensor (Casadio et al., 2012) and

109   this leads to the exclusion of much of Nigeria where that source is particularly large and urban

110   and industrial sources may contribute as well (Marais et al., 2014).

111   Marais et al. (2012) thus obtained a 2005-2009 monthly data set of vertical HCHO

112   columns with 1×1° spatial resolution screened against biomass burning and anthropogenic

113   influences and thus attributable to isoprene emissions (Fig. 1, left panel). They used GEOS-

114   Chem to derive the sensitivity, S, of the HCHO column (Ω_{HCHO}) at 12-15 LT to a perturbation Δ

115   in isoprene emission ($S = \Delta\Omega_{HCHO}/ \Delta E_{ISOP}$). Values of S increase linearly with NO_x under low-

116   NO_x conditions (boundary-layer NO_x < 500 pptv) and remain constant above 500 pptv NO_x. The

117   local regime for individual scenes was determined from concurrent observations of OMI

118   tropospheric NO_2 columns. Scenes affected by smearing (displacement of HCHO from the

119   isoprene emission source) were diagnosed with anomalously high values of S and excluded from

120   the data set. See Marais et al. (2012) for further details.

121   Marais et al. (2012) obtained in this manner a monthly isoprene emission inventory for

122   2005-2009 on a 1×1º grid (Fig. 1, center panel). The OMI overpass is at 13:30 LT and the

123   corresponding isoprene emissions are for 12-15 LT, typically the diurnal maximum. Also shown

124   in Fig. 1 is the MODIS IGBP land cover map (Friedl et al., 2002). Dominant vegetation types in

125   Africa are roughly defined by latitudinal bands, with evergreen (broadleaf) trees along the

126   Equator successively transitioning to the north and south to woody savannas (30-60% tree

127   coverage), savannas (10-30%), grasslands, and deserts. The HCHO column data follow this

128   vegetation gradient and so do the inferred isoprene emissions.

129   Marais et al. (2012) presented a detailed error characterization of their OMI-derived

130   isoprene emissions. Spectral fitting of the HCHO column has an error standard deviation of 8 ×

131   10^{15} molecules cm^{-2} for individual observations. Relating the fitted slant HCHO columns to

6

132   isoprene emissions incurs errors in the AMF estimate (20%), the isoprene oxidation mechanism

133   (15%), the use of OMI NO_2 to obtain S under low-NO_x conditions (20-40%), and smearing (30%

134   for high-NO_x conditions, 30-70% for low-NO_x). The resulting error in isoprene emission

135   estimates for individual scenes, adding in quadrature all error contributions, is 40% for high-NO_x

136   conditions and 40-90% for low-NO_x (Marais et al., 2012). A monthly mean estimate for a 1×1°

137   gridsquare typically averages 3000 individual scenes. Averaging reduces the error though only to

138   the extent that the error components are random.

139

140   **3. Evaluation with canopy flux measurements**

141   Canopy-scale isoprene flux measurements by relaxed-eddy accumulation (REA) are

142   available from a few African field campaigns (Table 1a). Figure 2 compares OMI-derived

143   isoprene emissions to REA measurements over equatorial evergreen trees (Greenberg et al.,

144   1999; Serça et al., 2001), woody savannas (Greenberg et al., 1999), and savannas (Harley et al.,

145   2003) in central and southern Africa (sites 1-4 in Fig. 1 and Table 1a). Also shown are the values

146   calculated using Eq. (1) with MEGAN v2.1 emission factors, combined Terra and Aqua MODIS

147   LAI (Yang et al., 2006), and the Goddard Earth Observing System (GEOS-5) assimilated

148   meteorological data. The Serça et al. (2001) and Harley et al. (2003) measurements (sites 1 and

149   4) are from walk-up towers with a flux footprint of about 600 m, while the Greenberg et al.

150   (1999) measurements (sites 2 and 3) are from aircraft with a flux footprint of ~100×100 km^2 at

151   site 2 and 30×30 km^2 at site 3. All values in Fig. 2 are for 12-15 LT. REA fluxes at sites 2-3,

152   obtained in the morning (9:30-11:30), are increased by a factor of 1.4 as a diurnal correction for

153   temperature and PAR following MEGAN.

154   No correction is applied to the REA flux measurements to account for interannual

155   variability between 1996 (sites 1-3), 2001 (site 4), and the satellite observation period (2005-

156   2009). As will be discussed in Sect. 4, temperature is the dominant modulator of isoprene

157   emissions in Africa and it does not drive significant interannual variability except in northern

158   savannas in August (not represented in Fig. 2).

159   OMI and MEGAN are sampled for the 1×1° gridsquare coincident with the observation

160   site and for the corresponding months. Interannual variability is of similar magnitude in the

161   OMI-derived and MEGAN data at sites 1 (November), 2 and, 3 where multi-year OMI data are

162   available. The variability is driven in MEGAN predominantly by temperature. At site 3 there are

163   no OMI data in the months of observation (November-December) because of biomass burning

164   interference and we show instead OMI-derived emissions in September-October, which should

165   be similar to November-December at this site according to MEGAN.

166   For the equatorial evergreen tree sites in central Africa (sites 1 and 2) OMI-derived

167   isoprene emissions are on average 2 times higher than the REA measurements and MEGAN is 5

168   times higher. The flux tower sampled vegetation with a relatively low fraction of isoprene

169   emitters. Nearby landscapes include monodominant stands of the *Gilbertiodendron* trees that

170   have a high isoprene emission factor (Serça et al., 2001). The distribution of this tree species

171   beyond the sampling domain is uncertain and application of its emission factor to land cover in

172   equatorial Africa contributes to the overestimate in MEGAN. OMI and MEGAN reproduce the

173   March-November decline at site 1 and this is driven in MEGAN by temperature.

174   Fluxes at site 2, where the REA sampling footprint is similar to OMI, have large spatial

175   variability implying that differences in the sampling footprint contribute to discrepancies at other

176   sites. Greenberg et al. (1999) applied a positive correction of ~20% to flux measurements at sites

8

177 2-3 to account for the transport of isoprene that was not accumulated in the two REA reservoirs.

178 A similar negative bias may affect measurements at sites 1 and 4 but the reported values have not

179 been adjusted. The aircraft REA measurements (sites 2 and 3) may have an additional negative

180 bias of ~25% due to the vertical flux divergence between the measurement altitude and the

181 surface (Karl et al., 2013).

182   At the woody savanna site OMI is 2.2 times higher than the REA measurement (1.8 times

183 higher if a 25% upward correction is applied to the REA measurement), while MEGAN is 8

184 times higher. At the savanna site OMI is 1.3 times higher than the REA flux measurement while

185 MEGAN is 2.4 times higher. The discrepancy at site 4 is partly due to the low (<10%) proportion

186 of isoprene emitting vegetation within the flux tower footprint as compared to ~35% for

187 savannas surveyed at surrounding field sites (Harley et al., 2003).

188   Overall the REA flux measurements indicate canopy-scale isoprene emissions that are

189 somewhat lower than derived from OMI and much lower than derived from MEGAN. As we

190 will show in Sect. 5, landscape-level isoprene emission factors measured during African field

191 campaigns are more consistent with OMI.

192

193 **4. Seasonality of isoprene emissions in Africa**

194   We examined the factors driving the seasonality of OMI-derived isoprene emissions,

195 focusing on three seasonally and ecologically coherent regions in Africa where emissions are

196 highest (Fig. 3): (1) equatorial forests dominated by tropical broadleaf evergreen trees, (2)

197 northern savannas (including woody), and (3) southern savannas (including woody). Figure 4

198 shows the seasonality of OMI-derived isoprene emissions for these three regions together with

199 MODIS LAI and GEOS-5 2-m air temperature. Isoprene emissions and 2-m temperature are for

200   12-15 LT and MODIS LAI is the combined Terra and Aqua product (Yang et al., 2006). Multi-

201   year averages (2005-2009) are shown; the regionally averaged interannual variability is small,

202   except over northern savannas in August as discussed below. Soil moisture and PAR are not

203   included in Fig. 4 as soil moisture only appears to affect southern savannas during the dry

204   season, and PAR in southern and northern savannas is convolved with temperature.

205   OMI-derived isoprene emissions for equatorial forests are a factor of 2 lower than

206   MEGAN and both show similar weak seasonality, with a decline from March to November that

207   is consistent with Serça et al. (2001) (Fig. 2) and is driven in MEGAN principally by

208   temperature. Although LAI exhibits similar seasonality, it remains above 3.5 m^2 m^{-2} year-round

209   and MEGAN is not sensitive to LAI values above 2-3 m^2 m^{-2} due to shading of lower-canopy

210   leaves (Guenther et al., 2006).

211   Availability of OMI-derived isoprene emission data for the northern savannas is limited

212   to April-November because of pervasive biomass burning influence during the December-March

213   dry season. Emissions are maximum in April, at the beginning of the wet season, and minimum

214   in August when the West African Monsoon (WAM) is fully developed over the continent

215   (Janicot et al., 2008) resulting in cooler temperatures. OMI-derived emissions largely follow

216   temperature over the April-November period. Year-to-year variability in the WAM affects

217   temperature in August, leading to interannual variability in August OMI isoprene emissions over

218   the 2005-2009 period that is correlated with temperature ($r = 0.55$).

219   The complete seasonality simulated by MEGAN in northern savannas shows low

220   isoprene emissions in the December-March dry season when LAI is less than 1 m^2 m^{-2}, and a

221   broad maximum in the April-November wet season as the August minimum in temperature is

222   compensated by a corresponding maximum in LAI. MODIS LAI in the northern savannas is less

223 than 2.5 m^2 m^{-2} year-round, sufficiently low that the MEGAN dependence on LAI does not

224 saturate (Guenther et al., 2012). However, MODIS may underestimate LAI in West Africa

225 during the wet season because of cloud contamination (Gessner et al., 2013).

226   OMI-derived emissions for southern savannas are in close agreement with MEGAN,

227 featuring a minimum in the winter dry season and a maximum in the summer wet season. The

228 seasonal minimum follows that of temperature (June-July) with a 1-month lag that reflects the

229 very dry conditions in July-September. We find that LAI and temperature are both important for

230 driving the seasonality of isoprene emissions in southern savannas.

231

232   **5. Satellite-derived isoprene emission factors for Africa**

233   The general ability of MEGAN to reproduce the seasonal variation of OMI-derived

234 isoprene emissions suggests that the MEGAN activity factors (γ in Eq. (1)) are appropriate for

235 conditions in Africa, with temperature and LAI as the principal drivers. The large MEGAN bias

236 over equatorial forests and northern savannas can therefore be attributed to an overestimate of

237 emission factors (E_o in Eq. (1)).

238   The emission factors in MEGAN represent isoprene fluxes for a canopy with leaves at

239 standard conditions of air temperature ($T = 303$ K) and light (PAR = 1000 μmol photons m^{-2} s^{-1}).

240 They are gridded using a detailed regional land cover map for Africa south of the Equator (Otter

241 et al., 2003) and the Olson et al. (2001) global ecoregion data in the north (Guenther et al., 2006).

242 Here we infer emission factors (E_0) from the OMI-derived canopy-level isoprene emission data

243 (E_{ISOP}) using Eq. (1). In so doing we only consider data with individual activity factors γ in the

244 range 0.5-1.5 so as to avoid errors driven by large departures from standard conditions.

245   Figure 5 shows the resulting distributions of MEGAN and OMI emission factors E_o over

246   Africa together with observations from the field campaigns of Table 1b. The latter are at the

247   landscape-level and were obtained by scaling measured leaf-level isoprene fluxes for

248   representative plant species with foliage density and species distribution data. Leaf-level

249   measurements at standard conditions were obtained by using enclosure measurements with

250   controlled temperature and PAR (Serça et al., 2001; Otter et al., 2002), or adjusting to standard

251   conditions with MEGAN activity factors for temperature and PAR (Guenther et al., 1996). For

252   the former an upward correction applied to the Serça et al. (2001) landscape emission factor

253   accounts for isoprene fluxes obtained from shade-adapted leaves that have lower emissions at

254   standard conditions than sunlit leaves (Guenther et al., 1999). Leaf-level fluxes of Klinger et al.

255   (1998) were determined to be at standard conditions with coincident measurements of

256   temperature and PAR, but we exclude the data from shaded leaves at dense forest sites.

257   We find from Fig. 5 remarkable agreement between OMI-derived emission factors and

258   the field data ($r = 0.55$, OMI normalized mean bias = -19%). Woody savannas in Zambia and

259   savannas in South Africa have large variability in E_o (0.5-4.5 mg C m^{-2} h^{-1}) that is reproduced by

260   OMI. The two sites in Botswana have low emission factors as the site to the north is dominated

261   by monoterpene emitting mopane vegetation, while the site to the south is predominantly

262   shrubland (Otter et al., 2002).

263   Differences between OMI and MEGAN emission factors are largest for equatorial

264   forests, and the field enclosure observations are in good agreement with OMI and much lower

265   than MEGAN. The equatorial forest enclosure measurements are used in MEGAN to estimate

266   emission factors there, but a large positive correction is applied to account for leaf enclosure

267   measurements of shade-adapted leaves. Our OMI-derived emission factors do not support such a

268   correction, and this is also reflected in the MEGAN overestimate of REA flux measurements

269   (Fig. 2). OMI emission factors for equatorial forests are larger in the west than east and this may

270   result from differences in the proportion of isoprene emitting species. The west is dominated by

271   dry tropical forests, while the east is dominated by permanently or seasonally flooded forests

272   (White, 1983).

273   Table 2 shows mean isoprene emission factors for individual PFTs as obtained by

274   mapping the data from Fig. 5 onto the MODIS IGBP land map (Fig. 1; Friedl et al., 2002) and

275   the Global Land Cover (GLC) 2000 land map (Mayaux et al., 2006). The distribution of MODIS

276   IGBP woody savannas is spatially consistent with GLC 2000 broadleaf trees and MODIS IGBP

277   savannas correspond to GLC 2000 shrubs interspersed with broadleaf trees and cultivated land.

278   The GLC 2000 classification scheme is more consistent with the PFTs of MEGANv2.1

279   (Guenther et al., 2012). OMI gives higher emission factors for forested vegetation than for

280   grasslands but the difference is not as large as MEGAN and more consistent with the field

281   enclosure observations. The largest differences between OMI and MEGAN emission factors are

282   for broadleaf evergreen trees and for semi-arid vegetation (shrubs and herbs).

283   The OMI-derived emission factors in Fig. 5 can be used to improve the MEGAN

284   isoprene emission estimates as computed from Eq. (1). Figure 6 compares the resulting isoprene

285   concentrations simulated by GEOS-Chem with a latitudinal profile of isoprene concentration

286   measurements below 1 km across West Africa during the AMMA wet season aircraft campaign

287   in July-August 2006 (Murphy et al., 2010). There is a strong vegetation gradient along the

288   AMMA flight track from the Gulf of Guinea to Benin woodlands to arid conditions in the north

289   that is reflected in the isoprene data. Simulated isoprene in GEOS-Chem is a factor of 2 too low

290   over Benin woodlands likely due to a seasonal low bias in MODIS LAI over West Africa from

291 cloud contamination (Gessner et al., 2013). Isoprene emissions over the AMMA domain are not

292 only sensitive to LAI, but also MEGAN emission factors (Ferreira et al., 2010). The OMI-

293 derived emission factors are much better able to reproduce the latitudinal gradient than the

294 original MEGAN emission factors, including in particular the decline to the north associated

295 with increased aridity. Throughout Africa MEGAN emission factors are too high for semi-arid

296 PFTs, as indicated by the overestimate in MEGAN for GLC 2000 sparse herb/shrub cover in

297 Table 2.

298

299 **6. Implications for oxidants and aerosols**

300   We use the GEOS-Chem chemical transport model to (1) evaluate the change in

301 atmospheric composition that results from replacing MEGAN emission factors with those

302 obtained using OMI, and (2) determine the impact of isoprene emissions on aerosols and

303 oxidants. GEOS-Chem includes the standard representation of oxidant-aerosol chemistry as

304 described for example by Mao et al. (2010) with updates to the isoprene oxidation (Paulot et al.,

305 2009a; 2009b).

306   Total annual isoprene emissions in Africa averaged over 2005-2009 using OMI-derived

307 emission factors are 77 Tg C a^{-1}, as compared to 104 Tg C a^{-1} in MEGAN v2.1. The difference is

308 mainly for the equatorial evergreen forest PFT in central Africa, where OMI-derived isoprene

309 emissions are 2-3 times lower than MEGAN. GEOS-Chem using OMI-derived isoprene

310 emissions indicates a factor of 4 increase in boundary layer OH concentrations over central

311 Africa relative to MEGAN, a 4 ppbv increase in surface O_3, and 8 ppbv decrease in surface

312 isoprene.

14

313   Figure 7 shows the effect of African isoprene emissions (using OMI-derived emission

314   factors) on surface concentrations of daily maximum 8-hour average (MDA8) O_3, particulate

315   matter (PM), NO_x, and OH. The largest effect on O_3 is over West Africa because of high

316   anthropogenic, soil, and biomass burning NO_x emissions (Marais et al., 2014). The largest effect

317   on PM is also over West Africa and reflects the availability of high pre-existing primary PM

318   from combustion (biomass burning and fuel) on which isoprene oxidation products can

319   condense. NO_x declines in West Africa and the tropics due to formation of isoprene nitrates.

320   Loss of OH from reaction with isoprene is highest in the tropics where low levels of NO_x limit

321   the recycling of HO_x radicals.

322

323   **7. Conclusions**

324   We used a 2005-2009 data set of monthly isoprene emissions in Africa derived from OMI

325   satellite observations of formaldehyde (HCHO) to study the factors controlling these emissions

326   in different areas of the continent. Our goal was to achieve a better representation of isoprene

327   emission in chemical transport models (CTMs), in part through evaluation and improvement of

328   the commonly used MEGAN emission inventory, and to examine the implications for oxidants

329   and aerosols over the continent.

330   We began by evaluating the OMI-derived isoprene emissions with relaxed-eddy

331   accumulation flux (REA) measurements obtained from above-canopy towers and aircraft during

332   African field campaigns. OMI-derived isoprene emissions are on average 2 times higher than

333   REA measurements over the equatorial forest and woody savannas but this could reflect biases in

334   the measurements. MEGAN emissions are 5-10 times higher.

335   We subdivided Africa into 3 seasonally and ecologically coherent regions to examine the

336   seasonality in OMI-derived isoprene emissions, and compare to the seasonality in MEGAN and

337   in driving environmental variables. Equatorial forests exhibit weak seasonality that is driven

338   predominantly by temperature, while seasonality in savannas is driven by both temperature and

339   LAI, in a manner consistent with MEGAN.

340   Isoprene emissions in MEGAN are computed as the product of (1) an emission factor E_o

341   characteristic of the PFT, (2) the LAI, and (3) activity factors dependent on local environmental

342   variables. We applied the LAI and MEGAN activity factors to our OMI-derived isoprene

343   emissions to obtain emission factors representative of different PFTs. These agree well with the

344   ensemble of leaf-level flux measurements in Africa and imply large downward corrections to

345   MEGAN emission factors for equatorial forests and semi-arid vegetation. Such corrections are

346   consistent with the latitudinal gradient of isoprene across West Africa measured in the AMMA

347   field campaign.

348   The OMI-derived emission factors can be incorporated into the MEGAN formalism (Eq.

349   (1)) to improve modeling of isoprene emissions in Africa. The resulting isoprene emissions for

350   the continent are 77 Tg C a^{-1}, as compared to 104 Tg C a^{-1} in the standard MEGAN inventory.

351   Most of the difference is over equatorial Africa. We conducted GEOS-Chem simulations with

352   and without African isoprene emissions (using OMI-derived emission factors) to examine the

353   impact on regional particulate matter (PM) and oxidants. The largest effect of isoprene emissions

354   on surface O_3 is over West Africa where NO_x is high, and the largest effect on PM is also over

355   West Africa because of pre-existing high concentrations of primary PM from combustion.

356

362

References:

Barkley, M. P., Palmer, P. I., Kuhn, U., Kesselmeier, J., Chance, K., Kurosu, T. P., Martin, R. V., Helmig, D., and Guenther, A.: Net ecosystem fluxes of isoprene over tropical South America inferred from Global Ozone Monitoring Experiment (GOME) observations of HCHO columns, J. Geophys. Res., 113, D20304, doi:10.1029/2008JD009863, 2008.

Barkley, M. P., Palmer, P. I., De Smedt, I., Karl, T., Guenther, A., and Van Roozendael, M.: Regulated large-scale annual shutdown of Amazonian isoprene emissions?, Geophys. Res. Lett., 36, L04803, doi:10.1029/2008GL036843, 2009.

Casadio, S., Arino, O., and Serpe, D.: Gas flaring monitoring from space using the ATSR instrument series, Remote Sens. Environ., 116, 239–249, doi:10.1016/j.rse.2010.11.022, 2012.

Claeys, M., Graham, B., Vas, G., Wang, W., Vermeylen, R., Pashynska, V., Cafmeyer, J., Guyon, P., Andreae, M. O., Artaxo, P., and Maenhaut, W.: Formation of secondary organic aerosols through photooxidation of isoprene, Science, 303, 1173–1176, doi:10.1126/science.1092805, 2004.

Curci, G., Palmer, P. I., Kurosu, T. P., Chance, K., and Visconti, G.: Estimating European volatile organic compound emissions using satellite observations of formaldehyde from the Ozone Monitoring Instrument, Atmos. Chem. Phys., 10, 11501–11517, doi:10.5194/acp-10-11501-2010, 2010.

Dufour, G., Wittrock, F., Camredon, M., Beekmann, M., Richter, A., Aumont, B., and Burrows, J. P.: SCIAMACHY formaldehyde observations: constraint for isoprene emission estimates over Europe?, Atmos. Chem. Phys., 9, 1647–1664, doi:10.5194/acp-9-1647-2009, 2009.

Ferreira, J., Reeves, C. E., Murphy, J. G., Garcia-Carreras, L., Parker, D. J., and Oram, D. E.: Isoprene emissions modelling for West Africa: MEGAN model evaluation and sensitivity analysis, Atmos. Chem. Phys., 10, 8453–8467, doi:10.5194/acp-10-8453-2010, 2010.

Friedl, M. A., McIver, D. K., Hodges, J. C. F., Zhang, X. Y., Muchoney, D., Strahler, A. H., Woodcock, C. E., Gopal, S., Schneider, A., Cooper, A., Baccini, A., Gao, F., and Schaaf, C.: Global land cover mapping from MODIS: algorithms and early results, Remote Sens. Environ., 83, 287–302, 2002.

Fu, T.-M., Jacob, D. J., Palmer, P. I., Chance, K., Wang, Y. X., Barletta, B., Blake, D. R., Stanton, J. C., and Pilling, M. J.: Space-based formaldehyde measurements as constraints on volatile organic compound emissions in east and south Asia and implications for ozone, J. Geophys. Res., 112, D06312, doi:10.1029/2006JD007853, 2007.

399   Gessner, U., Niklaus, M., Kuenzer, C., and Dech, S.: Intercomparison of leaf area index products
400   for a gradient of sub-humid to arid environments in West Africa, Remote Sens., 5,
401   1235-1257, doi:10.3390/rs5031235, 2013.

402   Greenberg, J. P., Guenther, A. B., Madronich, S., Baugh, W., Ginoux, P., Druilhet, A., Delmas,
403   R., and Delon, C.: Biogenic volatile organic compound emissions in central Africa
404   during the Experiment for the Regional Sources and Sinks of Oxidants (EXPRESSO)
405   biomass burning season, J. Geophys. Res., 104, D23, 30659–30671,
406   doi:10.1029/1999JD900475, 1999.

407   Guenther, A., Hewitt, C. N., Erickson, D., Fall, R., Geron, C., Graedel, T., Harley, P., Klinger,
408   L., Lerdau, M., McKay, W. A., Pierce, T., Scholes, B., Steinbrecher, R., Tallamraju, R.,
409   Taylor, J., and Zimmerman, P.: A global model of natural volatile organic compound
410   emissions, J. Geophys. Res., 100, D5, 8873–8892, doi:10.1029/94JD02950, 1995.

411   Guenther, A., Otter, L., Zimmerman, P., Greenberg, J., Scholes, R., and Scholes, M.: Biogenic
412   hydrocarbon emissions from southern African savannas, J. Geophys. Res., 101, D20,
413   25859–25865, doi:10.1029/96JD02597, 1996.

414   Guenther, A., Baugh, B., Brasseur, G., Greenberg, J., Harley, P., Klinger, L., Serça, D., and
415   Vierling, L.: Isoprene emission estimates and uncertainties for the Central African
416   EXPRESSO study domain, J. Geophys. Res., 104, D23, 30625-30639,
417   doi:10.1029/1999JD900391, 1999.

418   Guenther, A., Karl, T., Harley, P., Wiedinmyer, C., Palmer, P. I., and Geron, C.: Estimates of
419   global terrestrial isoprene emissions using MEGAN (Model of Emissions of Gases and
420   Aerosols from Nature), Atmos. Chem. Phys., 6, 3181–3210, doi:10.5194/acp-6-3181-
421   2006, 2006.

422   Guenther, A. B., Jiang, X., Heald, C. L., Sakulyanontvittaya, T., Duhl, T., Emmons, L. K., and
423   Wang, X.: The Model of Emissions of Gases and Aerosols from Nature version 2.1
424   (MEGAN2.1): an extended and updated framework for modeling biogenic emissions,
425   Geosci. Model Dev., 5, 1471-1492, doi:10.5194/gmd-5-1471-2012, 2012.

426   Harley, P., Otter, L., Guenther, A., and Greenberg, J.: Micrometeorological and leaf-level
427   measurements of isoprene emissions from a southern African savanna, J. Geophys.
428   Res., 108, D13, 8468, doi:10.1029/2002JD002592, 2003.

429   Janicot, S., Thorncroft, C. D., Ali, A., Asencio, N., Berry, G., Bock, O., Bourles, B., Caniaux,
430   G., Chauvin, F., Deme, A., Kergoat, L., Lafore, J.-P., Lavaysse, C., Lebel, T.,
431   Marticorena, B., Mounier, F., Nedelec, P., Redelsperger, J.-L., Ravegnani, F., Reeves,
432   C. E., Roca, R., de Rosnay, P., Schlager, H., Sultan, B., Tomasini, M., Ulanovsky, A.,
433   and ACMAD forecasters team: Large-scale overview of the summer monsoon over
434   West Africa during the AMMA field experiment in 2006, Ann. Geophys., 26, 2569–
435   2595, doi:10.5194/angeo-26-2569-2008, 2008.

436   Karl, T., Misztal, P. K., Jonsson, H. H., Shertz, S., Goldstein, A. H., and Guenther, A. B.:
437   Airborne flux measurements of BVOCs above Californian oak forests: Experimental

438   investigation of surface and entrainment fluxes, OH densities and Dahmköhler
439   numbers, *J. Atmos. Sci.,* 70, 3277-3287, doi:10.1175/JAS-D-13-054.1, 2013.

440 Klinger, L. F., Greenberg, J., Guenther, A., Tyndall, G., Zimmerman, P., M'Bangui, M.,
441   Moutsamboté, J.-M., and Kenfack, D.: Patterns in volatile organic compound emissions
442   along a savanna-rainforest gradient in central Africa, J. Geophys. Res., 103, D1, 1443–
443   1454, doi:10.1029/97JD02928, 1998.

444 Lelieveld, J., Butler, T. M., Crowley, J. N., Dillon, T. J., Fischer, H., Ganzeveld, L., Harder, H.,
445   Lawrence, M. G., Martinez, M., Taraborrelli, D., and Williams, J.: Atmospheric
446   oxidation capacity sustained by a tropical forest, Nature, 452, 737–740,
447   doi:10.1038/nature06870, 2008.

448 Levelt, P. F., van den Oord, G. H. J., Dobber, M. R., Mälkki, A., Visser, H., de Fries, J.,
449   Stammes, P., Lundell, J. O. V., and Saari, H.: The Ozone Monitoring Instrument, IEEE
450   T. Geosci. Remote Sens., 44, 1093–1101, doi:10.1109/TGRS.2006.872333, 2006.

451 Mao, J., Jacob, D. J., Evans, M. J., Olson, J. R., Ren, X., Brune, W. H., St. Clair, J. M., Crounse,
452   J. D., Spencer, K. M., Beaver, M. R., Wennberg, P. O., Cubison, M. J., Jimenez, J. L.,
453   Fried, A., Weibring, P., Walega, J. G., Hall, S. R., Weinheimer, A. J., Cohen, R. C.,
454   Chen, G., Crawford, J. H., McNaughton, C., Clarke, A. D., Jaeglé, L., Fisher, J. A.,
455   Yantosca, R. M., Le Sager, P., and Carouge, C.: Chemistry of hydrogen oxide radicals
456   (HO_x) in the Arctic troposphere in spring, Atmos. Chem. Phys., 10, 5823–5838,
457   doi:10.5194/acp-10-5823-2010, 2010.

458 Marais, E. A., Jacob, D. J., Kurosu, T. P., Chance, K., Murphy, J. G., Reeves, C., Mills, G.,
459   Casadio, S., Millet, D. B., Barkley, M. P., Paulot, F., and Mao, J.: Isoprene emissions in
460   Africa inferred from OMI observations of formaldehyde columns, Atmos. Chem. Phys.,
461   12, 6219-6235, doi:10.5194/acp-12-6219-2012, 2012.

462 Marais, E. A., Jacob, D. J., Wecht, K., Zhang, L., Yu, K., Lerot, C., Kurosu, T. P., and Chance,
463   K.: Anthropogenic emissions in Nigeria and implications for ozone air quality: a view
464   from space, Submitted to Atmos. Environ. (*in review*), 2014.

465 Mayaux, P., Eva, H., Gallego, J., Strahler, A. H., Herold, M., Agrawal, S., Naumov, S., De
466   Miranda, E. E., Di Bella, C. M., Ordoyne, C., Kopin, Y., and Roy, P. S.: Validation of
467   the Global Land Cover 2000 map, IEEE T. Geosci. Remote Sens., 44, 1728-1739, doi:
468   10.1109/TGRS.2006.864370, 2006.

469 Millet, D. B., Jacob, D. J., Boersma, K. F., Fu, T.-M., Kurosu, T. P., Chance, K., Heald, C. L.,
470   and Guenther, A.: Spatial distribution of isoprene emissions from North America
471   derived from formaldehyde column measurements by the OMI satellite sensor, J.
472   Geophys. Res., 113, D02307, doi:10.1029/2007JD008950, 2008.

473 Murphy, J. G., Oram, D. E., and Reeves, C. E.: Measurements of volatile organic compounds
474   over West Africa, Atmos. Chem. Phys., 10, 5281–5294, doi:10.5194/acp-10-5281-
475   2010, 2010.

Olivier, J. G. J., Bouwman, A. F., van der Maas, C. W. M., Berdowski, J. J. M., Veldt, C., Bloos, J. P. J., Visschedijk, A. J. H., Zandveld, P. Y. J., and Haverlag, J. L.: Description of EDGAR Version 2.0: A set of global emission inventories of greenhouse gases and ozone-depleting substances for all anthropogenic and most natural sources on a per country basis and on 1×1° grid, Bilthoven, The Netherlands., 1996.

Olson, D. M., Dinerstein, E., Wikramanayake, E. D., Burgess, N. D., Powell, G. V. N., Underwood, E. C., D'Amico, J. A., Itoua, I., Strand, H. E., Morrison, J. C., Loucks, C. J., Allnutt, T. F., Rickets, T. H., Kura, Y., Lamoreux, J. F., Wettengel, W. W., Hedao, P., and Kassem, K. R.: Terrestrial ecoregions of the world: a new map of life on earth, BioScience, 51, 933–938, 2001.

Otter, L. B., Guenther, A., and Greenberg, J.: Seasonal and spatial variations in biogenic hydrocarbon emissions from southern African savannas and woodlands, Atmos. Environ., 36, 4265–4275, 2002.

Otter, L., Guenther, A., Wiedinmyer, C., Fleming, G., Harley, P., and Greenberg, J.: Spatial and temporal variations in biogenic volatile organic compound emissions for Africa south of the equator, J. Geophys. Res., 108, D13, 8505, doi:10.1029/2002JD002609, 2003.

Palmer, P. I., Jacob, D. J., Chance, K., Martin, R. V., Spurr, R. J. D., Kurosu, T. P., Bey, I., Yantosca, R., Fiore, A., and Li, Q.: Air mass factor formulation for spectroscopic measurements from satellites: Application to formaldehyde retrievals from the Global Ozone Monitoring Experiment, J. Geophys. Res., 106, D13, 14539–14550, doi:10.1029/2000JD900772, 2001.

Palmer, P. I., Jacob, D. J., Fiore, A. M., Martin, R. V., Chance, K., and Kurosu, T. P.: Mapping isoprene emissions over North America using formaldehyde column observations from space, J. Geophys. Res., 108, D6, 4180, doi:10.1029/2002JD002153, 2003.

Palmer, P. I., Abbot, D. S., Fu, T.-M., Jacob, D. J., Chance, K., Kurosu, T. P., Guenther, A., Wiedinmyer, C., Stanton, J. C., Pilling, M. J., Pressley, S. N., Lamb, B., and Sumner, A. L.: Quantifying the seasonal and interannual variability of North American isoprene emissions using satellite observations of the formaldehyde column, J. Geophys. Res., 111, D12315, doi:10.1029/2005JD006689, 2006.

Paulot, F., Crounse, J. D., Kjaergaard, H. G., Kroll, J. H., Seinfeld, J. H., and Wennberg, P. O.: Isoprene photooxidation: new insights into the production of acids and organic nitrates, Atmos. Chem. Phys., 9, 1479–1501, doi:10.5194/acp-9-1479-2009, 2009a.

Paulot, F., Crounse, J. D., Kjaergaard, H. G., Kürten, A., St Clair, J. M., Seinfeld, J. H., and Wennberg, P. O.: Unexpected epoxide formation in the gas-phase photooxidation of isoprene, Science, 325, 730–733, doi:10.1126/science.1172910, 2009b.

Paulot, F., Henze, D. K., and Wennberg, P. O.: Impact of the isoprene photochemical cascade on tropical ozone, Atmos. Chem. Phys., 12, 1307-1325, doi:10.5194/acp-12-1307-2012, 2012.

514 Pfister, G. G., Emmons, L. K., Hess, P. G., Lamarque, J.-F., Orlando, J. J., Walters, S., Guenther,
515   A., Palmer, P. I., and Lawrence, P. J.: Contribution of isoprene to chemical budgets: A
516   model tracer study with the NCAR CTM MOZART-4, J. Geophys. Res., 113, D05308,
517   doi:10.1029/2007JD008948, 2008.

518 Ren, X., Olson, J. R., Crawford, J. H., Brune, W. H., Mao, J., Long, R. B., Chen, Z., Chen, G.,
519   Avery, M. A., Sachse, G. W., Barrick, J. D., Diskin, G. S., Huey, L. G., Fried, A.,
520   Cohen, R. C., Heikes, B., Wennberg, P. O., Singh, H. B., Blake, D. R., and Shetter, R.
521   E.: HO_x chemistry during INTEX-A 2004: Observation, model calculation, and
522   comparison with previous studies, J. Geophys. Res., 113, D05310,
523   doi:10.1029/2007JD009166, 2008.

524 Serça, D., Guenther, A., Klinger, L., Vierling, L., Harley, P., Druilhet, A., Greenberg, J., Baker,
525   B., Baugh, W., Bouka-Biona, C., and Loemba-Ndembi, J.: EXPRESSO flux
526   measurements at upland and lowland Congo tropical forest site, Tellus B, 53, 220–234,
527   2001.

528 Sharkey, T. D., and Yeh, S.: Isoprene emission from plants, Annu. Rev. Plant Physiol. Plant Mol.
529   Biol., 52, 407-436, 2001.

530 Shim, C., Wang, Y., Choi, Y., Palmer, P. I., Abbot, D. S., and Chance, K.: Constraining global
531   isoprene emissions with Global Ozone Monitoring Experiment (GOME) formaldehyde
532   column measurements, J. Geophys. Res., 110, D24301, doi:10.1029/2004JD005629,
533   2005.

534 Spurr, R. J. D., Kurosu, T. P., and Chance, K. V.: A linearized discrete ordinate radiative transfer
535   model for atmospheric remote-sensing retrieval, J. Quant. Spectrosc. Ra., 68, 689–735,
536   2001.

537 Stavrakou, T., Müller, J.-F., De Smedt, I., Van Roozendael, M., van der Werf, G. R., Giglio, L.,
538   and Guenther, A.: Evaluating the performance of pyrogenic and biogenic emission
539   inventories against one decade of space-based formaldehyde columns, Atmos. Chem.
540   Phys., 9, 1037–1060, doi:10.5194/acp-9-1037-2009, 2009a.

541 Stavrakou, T., Müller, J.-F., De Smedt, I., Van Roozendael, M., van der Werf, G. R., Giglio, L.,
542   and Guenther, A.: Global emissions of non-methane hydrocarbons deduced from
543   SCIAMACHY formaldehyde columns through 2003-2006, Atmos. Chem. Phys., 9,
544   3663-3679, doi:10.5194/acp-9-3663-2009, 2009b.

545 Torres, O., Tanskanen, A., Veihelmann, B., Ahn, C., Braak, R., Bhartia, P. K., Veefkind, P., and
546   Levelt, P.: Aerosols and surface UV products from Ozone Monitoring Instrument
547   observations: An overview, J. Geophys. Res., 112, D24S47,
548   doi:10.1029/2007JD008809, 2007.

549 Trainer, M., Williams, E. J., Parrish, D. D., Buhr, M. P., Allwine, E. J., Westberg, H. H.,
550   Fehsenfeld, F. C., and Liu, S. C.: Models and observations of the impact of natural
551   hydrocarbons on rural ozone, Nature, 329, 705–707, 1987.

552   White, F.: The Vegetation of Africa - a descriptive memoir to accompany the
553   UNESCO/AETFAT/UNSO vegetation map of Africa; Natural Resources Research
554   Report XX; U. N. Educational, Scientific and Cultural Organization, 356 pp., Paris,
555   1983.

556   Yang, W., Shabanov, N. V., Huang, D., Wang, W., Dickinson, R. E., Nemani, R. R.,
557   Knyazikhin, Y., and Myneni, R. B.: Analysis of leaf area index products from
558   combination of MODIS Terra and Aqua data, Remote Sens. Environ., 104, 297-312,
559   doi:10.1016/j.rse.2006.04.016, 2006.

560 **Tables**

561 Table 1a. Relaxed Eddy Accumulation (REA) isoprene flux measurements in Africa[a]

| Site[b] | Observation Period | | Platform | E_{ISOP} [10^{12} atoms C cm^{-2} s^{-1}][c] | Land Cover[d] | Reference |
	Date	Time				
1	Mar 1996	12-13 LT	tower	3.5	Equatorial trees	Serça et al. (2001)
	Nov 1996	12-13 LT		1.4		
2	Nov-Dec 1996	9:30-11:30 LT	aircraft	1.5	Equatorial trees	Greenberg et al. (1999)
3	Nov-Dec 1996	9:30-11:30 LT	aircraft	0.91	Woody savanna	Greenberg et al. (1999)
4	Feb 2001	12-13 LT	tower	1.2	Savanna	Harley et al. (2003)

562 [a]Data used to evaluate OMI-derived and MEGAN isoprene emissions (Fig. 2).

563 [b]See Fig. 1 for the location of each site.

564 [c]Mean values at 12-15 local time.

565 [d]MODIS IGBP land cover classification (Fig. 1).

566   Table 1b. Leaf-level isoprene flux measurements in Africa[a]

Site[b]	Observation Period	E_o [mg C m^{-2} h^{-1}]	Land Cover[c]	Reference
1	1996	3.6	Equatorial trees	Serça et al. (2001)
2	1995-1996	1.0	Equatorial trees	Klinger et al. (1998)
3	1995-1996	1.2	Woody savanna	Greenberg et al. (1999)
4	Feb 2001	0.47	Savanna	Harley et al. (2003)
	Dec 1992	2.4	Savanna	Guenther et al. (1996)
5	1995-1996	1.4	Woody savanna	Klinger et al. (1998)
6	1995-1996	3.0	Woody savanna	Klinger et al. (1998)
7	1995-1996	0.95	Savanna	Klinger et al. (1998)
8	Dec 1992	4.4	Savanna	Guenther et al. (1996)
	Feb-Mar 2001	4.5	Savanna	Otter et al. (2002)
9	Feb-Mar 2001	0.70	Shrubs	Otter et al. (2002)
10	Feb-Mar 2001	0.70	Savanna	Otter et al. (2002)
11	Feb-Mar 2001	8.2	Woody savanna	Otter et al. (2002)
	Feb-Mar 2001	3.6	Woody savanna	Otter et al. (2002)

567   [a]Emission factors E_o for standard conditions of temperature and PAR (Eq. (1)) used to compare to
568   MEGAN and OMI-derived values in Fig. 5.

569   [b]See Fig. 1 for the location of each site.

570   [c]MODIS IGBP land cover classification (Fig. 1).

571

572   Table 2. Isoprene emission factors for African plant functional types[a]

Plant functional type	Emission factor [mg C m^{-2} h^{-1}]	
	MEGAN	OMI
MODIS IGBP classification[b]		
Evergreen broadleaf trees	4.3 ± 2.0	2.7 ± 1.0
Deciduous broadleaf trees	4.4 ± 1.7	2.9 ± 0.2
Woody savannas	3.2 ± 1.3	2.6 ± 1.0
Savannas	2.9 ± 1.2	2.3 ± 0.8
Shrubs	3.0 ± 1.3	1.6 ± 0.8
Grasses	1.8 ± 0.9	1.6 ± 0.9
Crops	1.4 ± 0.9	1.6 ± 0.6
Mosaic of crops and natural vegetation	2.3 ± 1.1	2.5 ± 1.0
GLC 2000 classification[c]		
Evergreen broadleaf trees	4.4 ± 1.9	2.5 ± 1.0
Deciduous broadleaf trees	3.0 ± 1.3	2.7 ± 0.9
Shrubs	3.1 ± 1.6	2.2 ± 1.0
Herbs	2.4 ± 1.3	1.9 ± 0.9
Sparse herbs or shrubs	2.4 ± 1.2	1.5 ± 0.7
Cultivated land	1.8 ± 1.1	2.2 ± 0.9
Mosaic of crops and natural vegetation	3.0 ± 1.3	2.7 ± 0.7
Mosaic of crops and shrubs or grasses	2.6 ± 1.0	1.9 ± 0.9

573   [a] Isoprene emission factor E_o in Eq. (1) at standard conditions of air temperature (303 K) and
574   photosynthetically active radiation (1000 μmol photons m^{-2} s^{-1}). Values are means and standard
575   deviations obtained by mapping the E_o data from Fig. 5 onto the MODIS IGBP and GLC 2000
576   land maps. Plant functional type classifications are as given by each land map.

577   [b] Friedl et al. (2002) and shown in Fig. 1

578   [c] Mayaux et al. (2006)
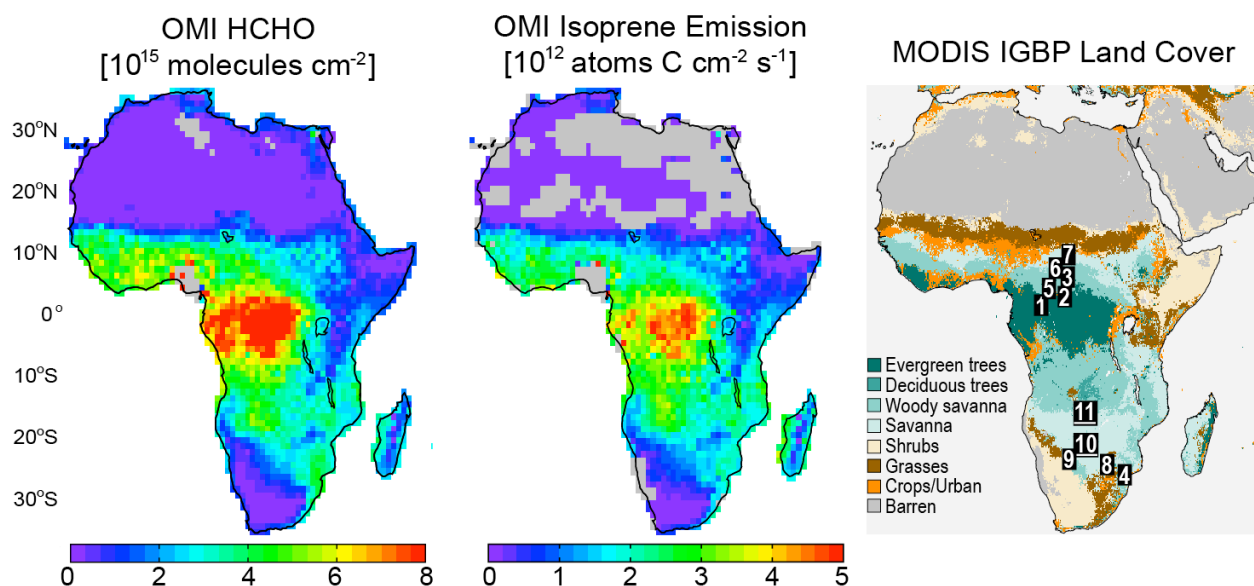
Figures

Figure 1. Annual mean (2005-2009) OMI HCHO vertical columns at 1×1° horizontal resolution screened against biomass burning and anthropogenic HCHO (left), and resulting OMI-derived isoprene emissions (center), as derived by Marais et al. (2012) and summarized in the text. The OMI observations are at 13:30 local time (LT) and the OMI-derived isoprene emissions are for 12-15 LT. The right panel is a MODIS IGBP land cover map (Friedl et al., 2002) with numbers showing the location of isoprene flux measurements used to evaluate the OMI-derived isoprene emissions (Tables 1a and 1b).
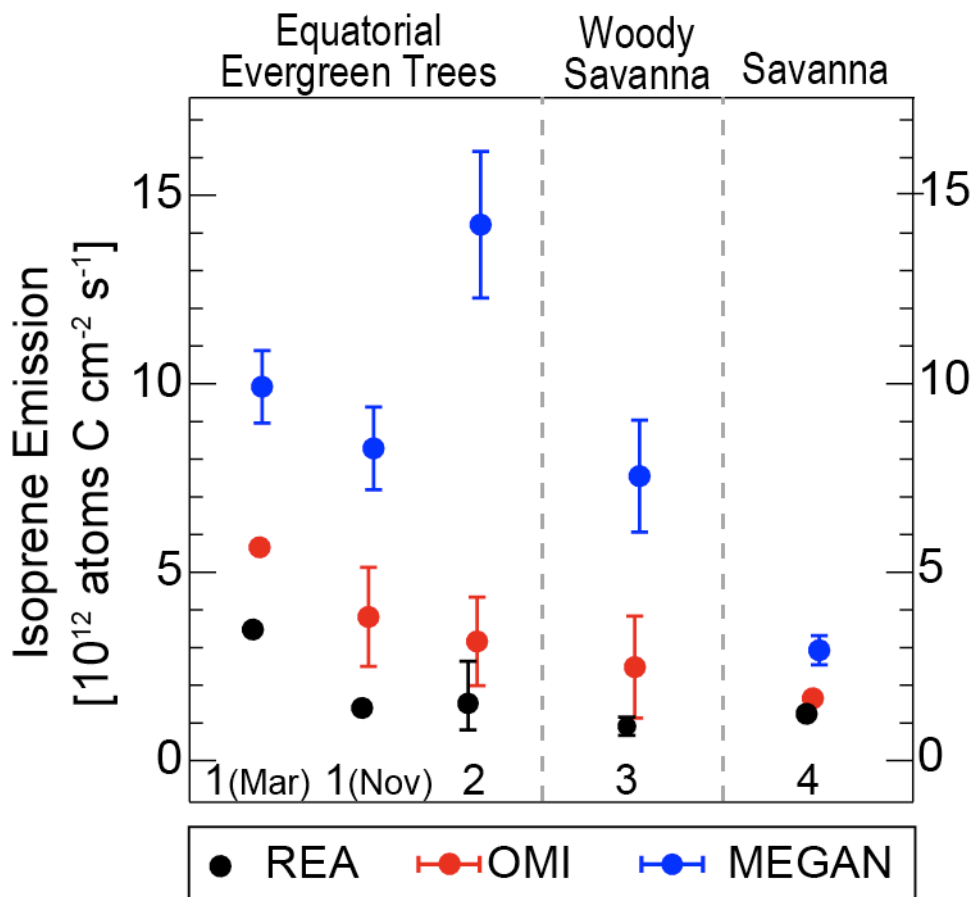
Figure 2. Mean canopy-scale isoprene emissions at African sites 1-4 (see Fig. 1 and Table 1a) measured by relaxed-eddy accumulation (REA), and comparison to OMI-derived and MEGAN values. All values are for 12-15 local time, with diurnal correction for REA measurements at sites 2 and 3 (see text). Vertical bars on the REA measurements for sites 2-3 are the interquartile ranges over the aircraft sampling domain given in Greenberg et al. (1999). OMI-derived and MEGAN values are 2005-2009 monthly averages for the site locations and observation times, with interannual standard deviations shown as vertical bars. Mar=March, Nov=November.

northern savannas

equatorial forests

southern savannas

600
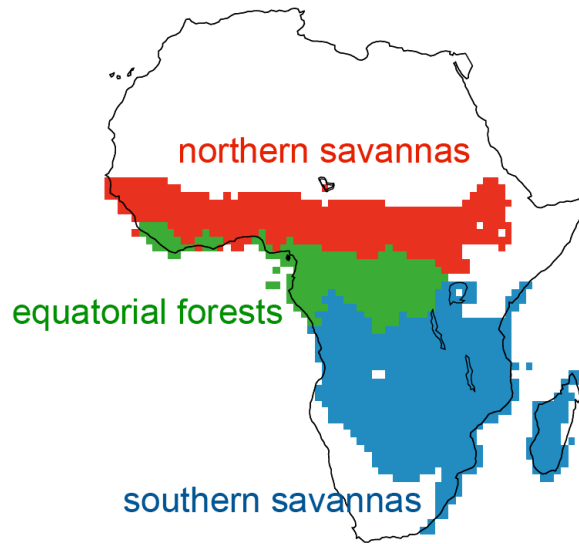
Figure 3. Coherent regions used for analysis of the factors controlling OMI-derived isoprene emissions. Land cover definitions are from the MODIS IGBP map (Fig. 1).

601

602

603
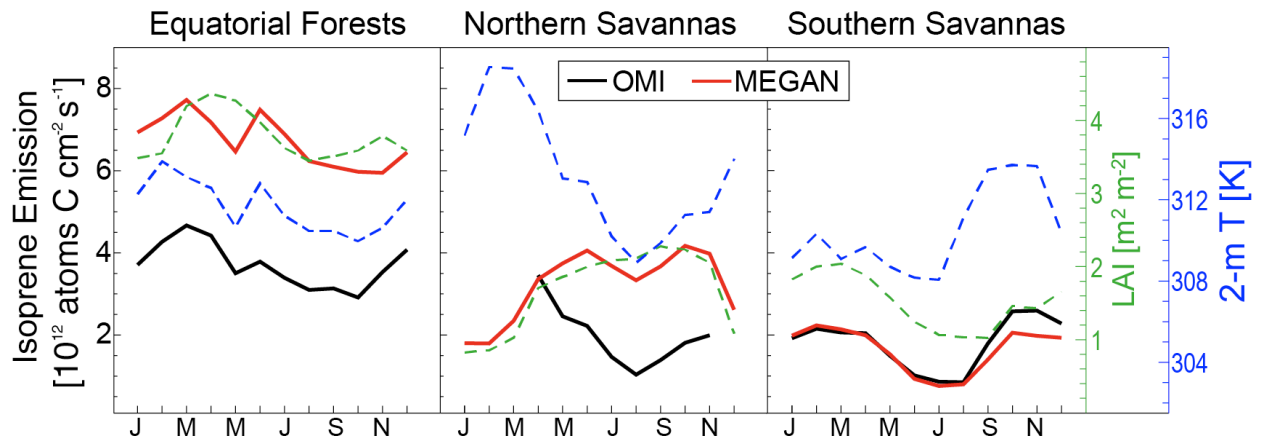
Figure 4. Seasonality of isoprene emissions and environmental variables averaged over the coherent African regions of Fig. 3. Monthly mean OMI-derived (black) and MEGAN (red) isoprene emissions are shown together with GEOS-5 2-m temperature (blue) and MODIS LAI (green). OMI-derived isoprene emissions are not available for northern savannas in December-March because of biomass burning interference. Emissions and 2-m temperature are for 12-15 local time. LAI is the combined Terra and Aqua product (Yang et al., 2006). All data are means for 2005-2009.
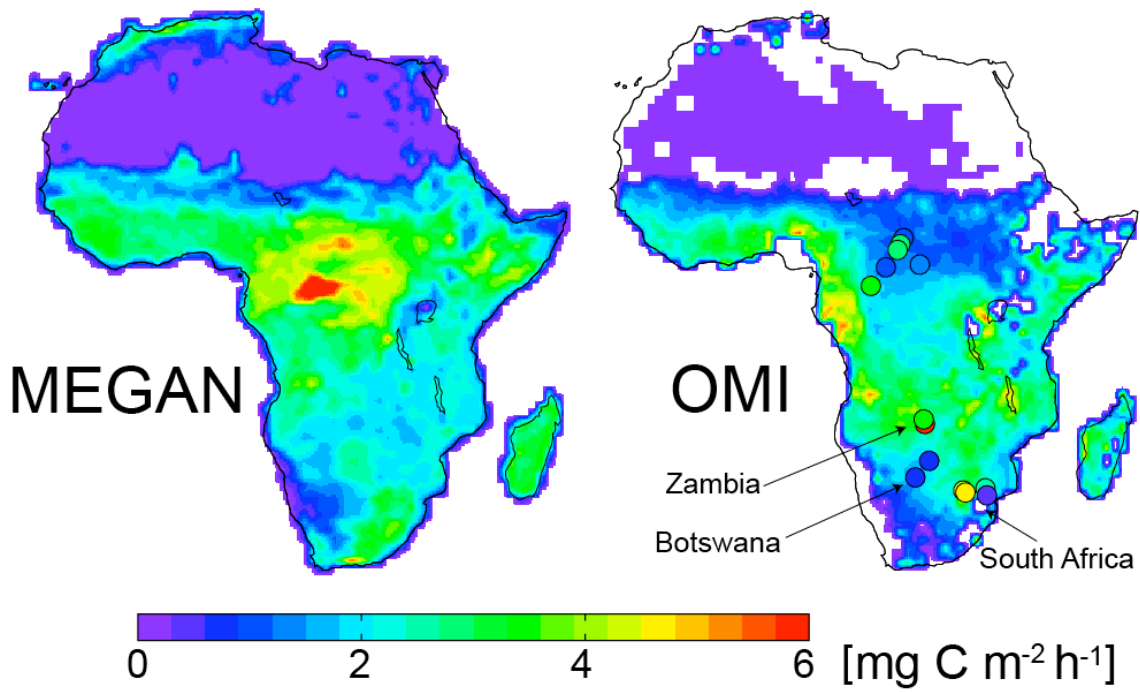
Figure 5. Isoprene emission factors (E_o in Eq. (1)) representing the emission flux under standard conditions. Measured landscape-level emission factors from field sites (circles; see Fig. 1 and Table 1b) are compared to those used in MEGAN (left) and obtained with OMI (right). White indicates missing OMI data.
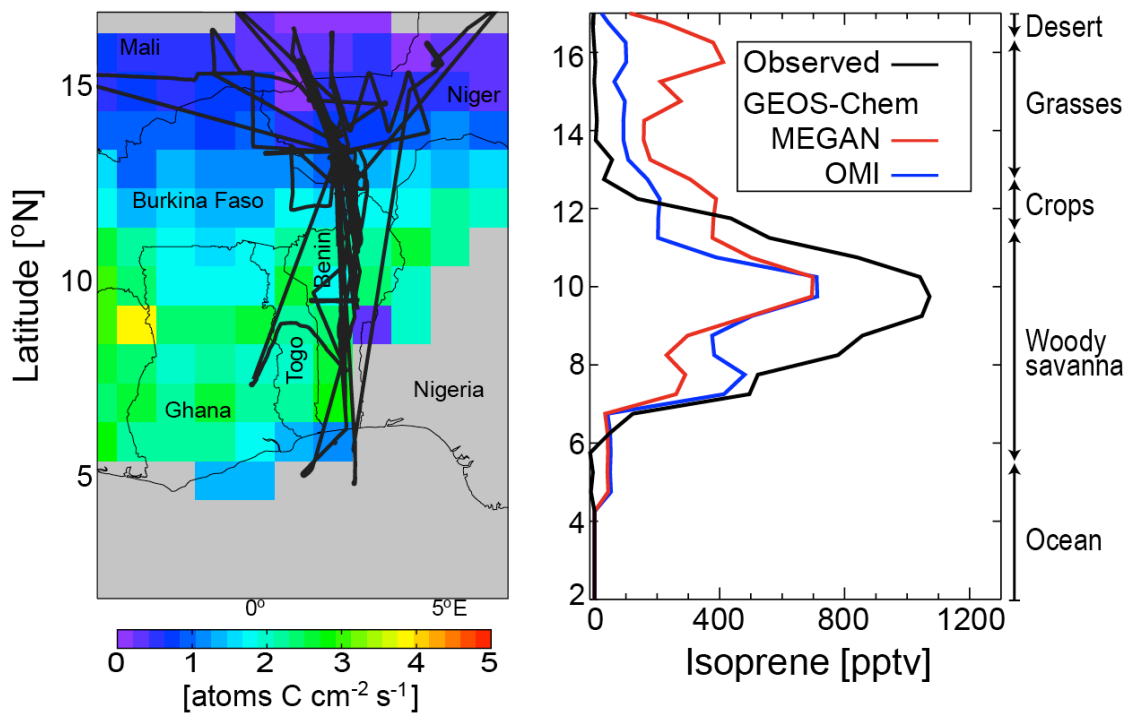
Figure 6. Latitudinal variability of isoprene in West Africa. Left panel shows the July-August 2006 AMMA flight tracks superimposed on July-August 2005-2009 OMI-derived isoprene emissions (Marais et al., 2012). Right panel shows boundary-layer (< 1 km) isoprene concentrations along the AMMA flight tracks; observations averaged over 0.5° latitude bands are compared to GEOS-Chem model results using either MEGAN or OMI-derived isoprene emission factors E_o. Dominant MODIS IGBP biomes along the flight tracks are indicated.
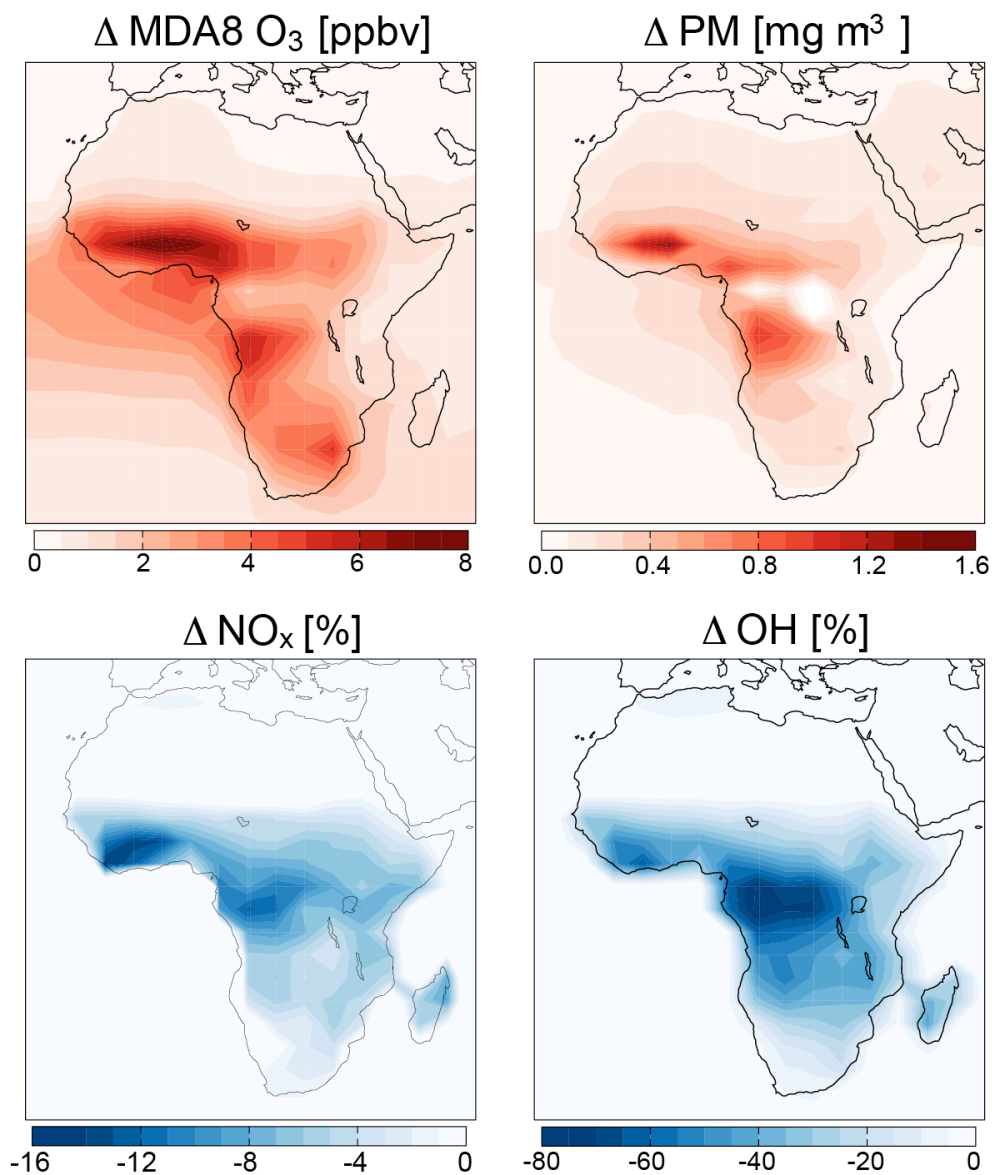
Figure 7. Effect of African isoprene emissions on regional oxidant and particulate matter (PM) concentrations in surface air. Shown are the annual mean differences Δ between GEOS-Chem simulations with and without African isoprene emissions. Isoprene emission is computed using OMI-derived emission factors.